In-vivo Brain Anatomical Connectivity Using Diffusion Magnetic Resonance Imaging and Fuzzy Connectedness

Stamatios N. Sotiropoulos, Christopher R. Tench and Li Bai

Abstract—**Diffusion-weighted (DW) magnetic resonance imaging is the only non-invasive and in-vivo method available for studying brain white matter anatomical connectivity. Tractography algorithms have been developed to reconstruct neuronal tracts utilizing DW images. In this study, a new tractography method is presented. This is based on a fuzzy framework, as suggested by the intrinsic fuzzy nature of medical images. The proposed technique checks all possible paths -defined on the discrete image grid- between any pair of voxels and assigns a connectivity value, representative of the strength of the strongest path. Path branching, which is not well captured by binary streamline techniques, is inherently considered. Compared to other distributed tractography approaches, our method combines a) converged connectivity values for all image voxels, b) connectivities that do not drop systematically with the distance from the seed, c) path propagation with relatively high angular resolution and d) fast execution times. Results are shown on both simulated and real images, where predicted tracts agree well with a-priori anatomical knowledge.**

I. Introduction

DIFFUSION-weighted (DW) magnetic resonance imaging (MRI) [1] utilizes as a contrast agent the random, thermally-driven motion of water molecules, known as diffusion. In living tissues water diffusion is hindered by the various micro-structural compartments, such as cell membranes. Particularly in tissues with coherent structure, this hindrance is systematic and diffusion profile appears anisotropic [2], i.e. there is a preference towards a specific direction. The high diffusion anisotropy exhibited in brain white matter (WM) is of particular interest, as it can be used to infer brain anatomical structure, non-invasively and in-vivo [3-5]. Under the assumption that diffusion is faster along than across neuronal axons, the direction of fastest diffusion coincides in many cases with the average WM fibre orientation in each image voxel [6]. Following these local fibre orientation estimates across the whole brain, WM tracts can be reconstructed and brain anatomical connectivity can be studied, through a process known as tractography [3, 4].

There are many techniques to process DW images and obtain fibre orientation estimates on a voxel by voxel basis (see [7, 8] for a review). The objective is to use a set of DW images to estimate in each voxel the probability density function (pdf) P of water diffusion displacements. The maxima of the angular profile of P will give fibre orientation estimates [7]. The most commonly used technique that will also be utilized in this study is diffusion tensor imaging (DTI) [6, 9]. The diffusion tensor model assumes that P is a zero-mean trivariate Gaussian and estimates the covariance matrix of this function [9]. A 3x3 symmetric, positive definite matrix (diffusion tensor) is computed in each voxel. The eigenvalues of this matrix provide the water diffusion coefficients along the three orthogonal orientations indicated by the respective eigenvectors [6]. The unit-normalized principal eigenvector, i.e. the one associated with the maximum eigenvalue, is used as an estimate of WM fibre orientation in the voxel of interest.

Early work on tractography was based on streamline-like algorithms, which attempted to propagate a curve through the vector field of principal eigenvectors [3, 4]. A starting (seed) point or starting region of interest (ROI) is defined and the algorithms reconstruct a path by following in space the fibre orientation estimates in each location of the image grid. Despite its success to delineate many major WM tracts [10], streamline tractography has two major limitations, which we are addressing here: a) there is no intrinsic way to provide a confidence measure of a reconstructed path, b) in the case of tract branching, propagation will continue only along one of the branches.

The importance of having a measure that characterizes how feasible the reconstructed tracts are stems from the fact that DW images are by nature fuzzy [11, 12]. Experimental noise, hardware limitations, partial volume artifacts and limited spatial resolution are some of the factors that contribute to the fuzziness of the images. Therefore, connectivity between voxels is not adequately described by "hard binary" relationships, as performed in streamline tractography, where a connection is assumed to either exist or not. Fuzzy statements should govern track delineation to address the inherent inaccuracies of the DW images [11].

Towards this direction, probabilistic tractography techniques [13, 14] compute indirectly an index of anatomical connectivity by extending the streamline

Manuscript received June 12, 2008. This work was supported by the European Commission Fp6 Marie Curie Action Programme (MEST-CT-2005-021170) under the CMIAG project.

S. N. Sotiropoulos is with the division of Clinical Neurology, University Hospital, University of Nottingham, Nottingham, NG7 2UH, UK (e-mail: msxss6@nottingham.ac.uk).

C. R. Tench is with the division of Clinical Neurology, University Hospital, University of Nottingham, Nottingham, NG7 2UH, UK (phone: +44 (0)115 823 1192; fax: +44 (0)115 970 9738; e-mail: Christopher.Tench@nottingham.ac.uk).

L. Bai is with the School of Computer Science & IT, University of Nottingham, Jubilee Campus, Nottingham, NG8 1BB, UK (e-mail:Bai.Li@ nottingham.ac.uk).

framework. These techniques capture the uncertainty in the fibre orientation estimate, by treating it as a random variable and defining a distribution for it. Streamline tractography is then performed, but for each propagation step a random sample is drawn from the orientation distribution defined at the current location. Many streamlines are generated from a seed point and the fraction of streamlines that pass through is defined as the index of connectivity of the specific voxel to the seed. A drawback of these techniques is the inevitable reduction of the connectivity index with distance from the seed [13, 14]. Moreover, the repetitive streamline generation increases execution time, while the connectivity values can depend on the total number of streamlines launched.

Front propagation algorithms attempt to overcome the limitations of streamline tractography by evolving a surface from the seed [15, 16]. Propagation is fastest along directions –normal to the surface- that are collinear with the fibre orientation estimates. In [15], the fast marching algorithm is used for front propagation. A map with front arrival times is calculated and tracts are generated in a backward fashion, from points of interest back to the seed, using gradient descent through the arrival times. In [16], an empirical orientation distribution function is used to drive the evolution of the front. In an iterative fashion, child fronts are generated by stepping away from parent points along the orientations of highest probability. These child fronts are merged to form a surface from which new child fronts will be generated.

In this study, we present a new fuzzy method for performing distributed brain tractography that is not based on streamline propagation. We introduce a modified version of the fuzzy connectedness algorithm [12]; initially proposed for image segmentation. Fuzzy connectedness tractography (FCT) assigns a global connectivity value between any pair of voxels, after searching exhaustively all possible paths that connect the two voxels on the discrete image grid and eventually finding the strongest. Compared to other distributed tractography methods, FCT provides in a single iteration converged connectivity values for all image voxels that do not drop systematically with the distance from the seed. Furthermore, path propagation is performed with relatively high angular resolution and combined in a single step with connectivity assignment. Algorithm implementation with dynamic programming allows execution at almost interactive speeds. The paper is organized as follows. In Section II, we give a brief overview of diffusion tensor imaging used to obtain fibre orientation estimates. Then, the fuzzy connectedness framework is presented. Modifications of the algorithm and adaptation to the tractography problem are described. Results that justify our method on simulated data and on human in-vivo MRI data are presented in Section III. Finally, current limitations and future work are discussed in Section IV. Preliminary results have been presented by the authors in abstract form [17].

II. THEORY AND METHODS

A. Diffusion Tensor Imaging

In diffusion tensor imaging (DTI) [6], the image intensity S_k for a given voxel, measured after the application of a diffusion-sensitizing magnetic field gradient is given by [9]:

$$S_k = S_o \cdot \exp(-b\boldsymbol{g_k}\boldsymbol{D}\boldsymbol{g_k^T}) \quad (1)$$

where S_o is the image intensity measured at the same voxel without a diffusion-sensitizing gradient, $\boldsymbol{g}_k$ is the orientation vector of the k-th diffusion-sensitizing gradient, b depends on the magnitude and duration of the gradient and $\boldsymbol{D}$ is the unknown diffusion tensor. This symmetric tensor has 6 elements, so at least 6 equations of the form (1) (i.e. $k \geq 6$ measurements) are needed to solve the system. Once the tensor $\boldsymbol{D}$ is calculated [9], it is diagonalized and its principal eigenvector provides an estimate of fibre orientation in the respective voxel.

B. Fuzzy Connectedness Framework

Given a 3-dimensional digital image, we describe each volume element (voxel) of the image as a vector containing the three cartesian coordinates of the voxel centre. We then define a local fuzzy relation between any two voxels **i** and **j** of the image called affinity. The strength of the affinity is given by the function $\mu(\mathbf{i},\mathbf{j})$, determined by the product of a) the similarity of the image intensities or some intensity-based features at **i** and **j** with b) the adjacency of the two voxels. Normally, the adjacency is a binary relationship with a value of 1 for neighbouring and 0 for non-neighbouring voxels. Therefore, non-neighbouring voxels have a zero affinity.

Given the local affinity relation, fuzzy connectedness (FC) assigns strengths $f(\mathbf{a},\mathbf{b})$ of a global fuzzy relation called connectedness between any pair of voxels **a** and **b**. The connectedness value is representative of the weakest link of the strongest path between **a** and **b**. There are many paths that connect **a** and **b** in the spatial grid of the image. Each path can be considered a chain of voxels, with successive elements being adjacent and directly connected to each other. In the FC framework, the smallest affinity μ along a path, i.e. the weakest link of the chain, determines the strength of the path. Considering all possible routes connecting **a** and **b**, the strength of the strongest path will be the connectedness $f(\mathbf{a},\mathbf{b})$. Therefore, after selecting a seed voxel, FC can compute a connectedness value between the seed and any other voxel in the image. The algorithm can be implemented using dynamic programming which allows execution at interactive speeds [18]. We should point out that both the fuzzy affinity and the connectedness strengths take values in the continuous interval [0,1].

C. Fuzzy Connectedness Tractography

The idea of trying all possible paths connecting two voxels, finding the strongest path based on affinity values,

and assigning a connectedness value between the two voxels of interest is attractive for brain tractography. In this study we use DTI to obtain local fibre orientation estimates. Thus, we utilize the principal eigenvector of the diffusion tensor to determine voxel similarity. The affinity function μ between neighbouring voxels **i** and **j** is a modified version of the voxel similarity function proposed in [15, 19]:

$$\mu(\mathbf{i},\mathbf{j}) = 1/\left[\Gamma\cdot\left(1-\min\left(\left|\mathbf{e}_1(\mathbf{i})\cdot\mathbf{n}(\mathbf{i},\mathbf{j})\right|,\left|\mathbf{e}_1(\mathbf{j})\cdot\mathbf{n}(\mathbf{i},\mathbf{j})\right|,\left|\mathbf{e}_1(\mathbf{i})\cdot\mathbf{e}_1(\mathbf{j})\right|\right)\right)\right] \quad (2)$$

where $\mathbf{e}_1(\mathbf{i})$ is the principal eigenvector of the diffusion tensor at voxel **i**, $\mathbf{n}(\mathbf{i},\mathbf{j})$ is the unit vector pointing from the centre of voxel **i** to the centre of voxel **j** and Γ a normalization constant to keep affinities in the [0,1] interval. The above function is peaked when all three vectors are collinear, i.e. when the eigenvector of voxel **i** points to the centre of voxel **j** and vice versa.

One would anticipate that incorporating the above affinity function to the FC algorithm and choosing a seed voxel or region of interest (ROI) would produce a tractography-like connectivity map. Doing so, however, does not produce desirable results. FC will try all possible routes between a voxel and the seed that are legal connections on the spatial grid of the image. However there is no guarantee that these routes will be *anatomically realistic*. Particularly, 180° turns are not inherently avoided by the FC algorithm. To get around such conditions we introduce a memory property for each voxel. Once a voxel **j** is identified as part of a path, its previous voxel **i** in the pathway chain, through which **j** is connected to the seed in a strongest way, is stored. This way, knowing the current and the previous voxel of a path, we can allow only forward path propagation.

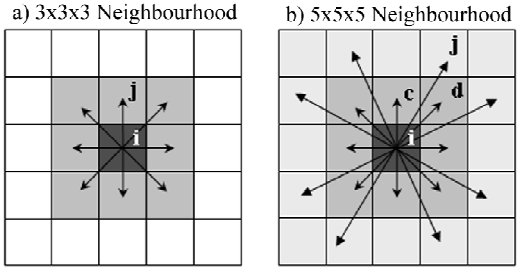

Fig. 1. Different neighbourhood systems of focal voxel **i**. Only neighbours within the same slice as **i** are presented. Black arrows represent candidate directions for path propagation. Half of these directions will be discarded using the memory property, so that only forward propagation occurs. Dark gray: focal voxel, intermediate gray: nearest neighbours, light gray: next nearest neighbours.

So far, the utilized neighbourhood size has not been defined. The number of neighbours of voxel **i** considered at each step will determine the number of candidate propagation directions. A straightforward implementation is to use the immediate 26 neighbours of each voxel, i.e. a 3x3x3 neighbourhood. This allows 45° steps between possible propagation directions. We can increase the angular resolution of path propagation, by increasing the neighbourhood size to 5x5x5 and include next nearest neighbours, 124 neighbours in 3D, as shown in Fig. 1. This will allow 22.5° steps. In this case, though, neighbours that are not directly connected to the focal voxel **i** exist, such as voxel **j** in Fig. 1b. To avoid discontinuities in paths, we require that at least one nearest neighbour of the focal voxel is included in the path. More specifically, for each next nearest neighbour **j** (light gray in Fig. 1b) we consider the two nearest neighbours **c** and **d** (intermediate gray in Fig. 1b) that are transversed by the vector connecting the focal voxel **i** to **j**. We require that the connectedness value of at least one of the voxels **c** and **d** is not smaller than the connectedness value of **j**.

The FC algorithm described in [18] is modified, as shown in the Appendix. The FC tractography (FCT) will output a map of fuzzy connectedness values between any voxel in the image and the seed voxel or seed ROI. In this study, we exclude from the algorithm voxels that have low diffusion anisotropy; assuming that these represent gray matter or CSF [5, 6]. In these regions, the fibre orientation estimates are not relevant [20]. We quantify diffusion anisotropy in each voxel using the fractional anisotropy (FA) index [5]:

$$\mathrm{FA} = \sqrt{\frac{3((\lambda_1-\lambda_{av})^2+(\lambda_2-\lambda_{av})^2+(\lambda_3-\lambda_{av})^2)}{2(\lambda_1^2+\lambda_2^2+\lambda_3^2)}} \quad (3)$$

where λ_i is the i-th eigenvalue of the diffusion tensor and λ_{av} is the average of the three eigenvalues. The FA is 0 for fully isotropic and 1 for infinitely anisotropic tensors.

An FA threshold of 0.2 is used to exclude voxels with too isotropic diffusion profile. For all other voxels, the algorithm will output a fuzzy connectedness value, describing the connectivity to the seed. By choosing the voxels with the highest FC values, we can identify regions that are more likely to be connected to the seed, given the chosen affinity function. The strongest paths underlying these connections can be found using backward propagation from the end points to the seed. Using the memory information, we can go from each voxel **j** back to its previous **i**, through which **j** is connected to the seed in a strongest way.

D. Simulations

A circular anisotropic phantom embedded in an isotropic medium was simulated (Fig. 2a). The trace of all diffusion tensors was 2.1×10^{-3} mm^2/sec, typical of brain tissue [6]. The FAs were 0.7 and 0.3 for the anisotropic and isotropic voxels respectively. Isotropic tensors had a random orientation. For the voxels belonging to the anisotropic circular ring, tensors had their principal eigenvector tangent to the circle passing from that point. Once the diffusion tensor in each voxel was chosen, noise-free DW MRI signals were then simulated as described in [21]. Then, zero-mean Gaussian noise was added in quadrature to simulate the Rician nature of MRI noise [21]. The signal to noise ratio (SNR) was defined as

the average intensity of the non-diffusion weighted image (S_o in (1)) divided by the standard deviation of the noise.

E. MRI Data Acquisition and Processing

A whole-brain data set was acquired, with local research ethics committee approval, from a healthy male subject who gave informed consent. Scans were performed using a single-shot, spin-echo, echo-planar, diffusion-weighted sequence [1] (acquisition matrix 112x112 with in-plane resolution 2x2 mm, interpolated during reconstruction to 224x224, TE=60 ms, TR=9500 ms) in a Philips 3T Achieva clinical imaging system. A parallel imaging factor of 2 was used. Three non-DW images were acquired and averaged. Diffusion weighting was applied along k=32 evenly spaced directions with b=1000 s/mm^2 [22]. 52 slices were acquired with a thickness of 2 mm.

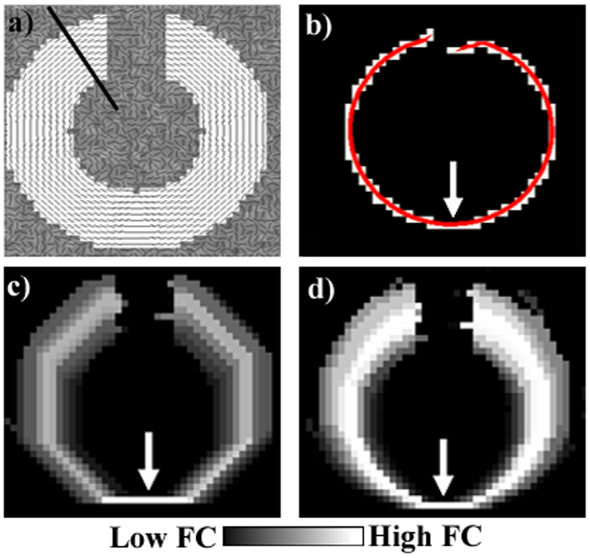

Fig. 2. Application of FCT to computer simulated data (SNR=15). a) Principal eigenvectors of a numerical phantom superimposed on an FA map, b) Streamline generated from a single seed voxel and corresponding binary connectivity index (white=connected, black=not connected), d) Fuzzy connectedness values obtained using a 3x3x3 (c) and 5x5x5 (d) neighborhood. Seed voxels are indicated with an arrow.

Images were corrected for eddy current distortion using an affine registration implemented in FSL's diffusion toolbox [15]. Brain was extracted from the images using the brain extraction tool [15]. To get isotropic voxels (1x1x1 mm^3) and visually smoother results, the brain volume was trilinearly interpolated along the out-of-plane- direction. A diffusion tensor model was then fitted in each voxel using a linear least squares approach [5, 9]. Each tensor was diagonalized and the principal eigenvector and the FA were calculated. For comparison purposes, streamline tractography was performed when necessary, using the algorithm of [3]. As noted before, streamline tractography propagates a curve within the vector field of fibre orientation estimates [3, 4]. Contrary to FCT, it does not necessarily connects voxel centres, allowing thus greater spatial continuity. However, in each propagation step, one of the available neighbours is selected and propagation continues only towards this neighbour.

III. Results

A. Simulations

We first applied FCT to the simulated anisotropic phantom. Fig. 2a shows the principal eigenvectors superimposed on FA values. Fig. 2c and 2d show the output of FCT when two different neighbourhood sizes are utilized. The gray scale corresponds to fuzzy connectedness values. For comparison, the binary connectivity index obtained from streamline tractography for the same seed is shown in Fig. 2b. The distributed nature of FCT compared to streamline tractography is evident. FCT identified strong paths arising from the seed, along with other weaker connections. The increased angular resolution provided by the larger neighbourhood is beneficial, since the discrete picture of Fig. 2d resembles more a circular tract. Furthermore, FC values are increased in the latter case, since smoother transitions were possible between neighbours. This increase is desirable, since in an ideal noise-free regime a straight path would have a connectedness of 1 along its length.

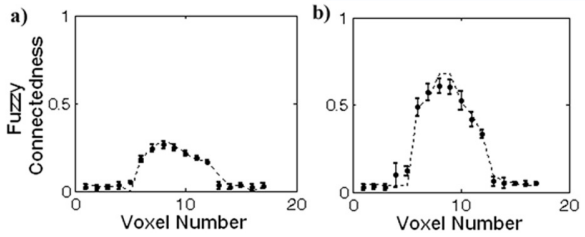

Fig. 3. Mean (circle) and standard deviation (horizontal bars) of fuzzy connectedness values across 100 simulations (SNR=15), at voxel locations defined by the linear ROI of Fig. 2a (black solid line). Voxel counting starts from the top left corner of the phantom and increases towards the phantom centre. FC values were obtained using a) a 3x3x3 neighbourhood, b) a 5x5x5 neighbourhood. Noise-free FC values are indicated by the dashed line.

To test the behavior of FCT against noise, 100 simulations were performed at a given SNR level in a Monte Carlo fashion, i.e. random Rician noise was added in each simulation. The ROI shown in Fig. 2a with a black solid line defined a cross-section of the phantom. The central part of this cross-section (7 voxels) was within the anisotropic circular ring, while its edges (5 voxels each) were within the isotropic region. The FC values at the voxels along this ROI were studied across the 100 simulations. Fig. 3 shows the mean (denoted by a circle) and the standard deviation (denoted by horizontal bars) of the FC values at each of these discrete voxel locations, using the 3x3x3 and the 5x5x5 neighbourhood. The noise-free FC values along the ROI are shown by a dashed line, which is continuous just for visualization purposes. The SNR in these simulations was 15, representative of the noise conditions in a DTI experiment. The plots show the robustness of the calculated FC values against noise and their good agreement with the

noise-free ones. Given that the simulated tract is very curved and that the affinity we use (2) penalizes curvature, it is expected that the connectedness of the stronger paths will be smaller than one. Deviation from this ideal value is reduced in the case of the large neighbourhood (Fg. 3b). Compared to the values obtained with a small neighbourhood (Fig. 3a), the connectedness of the voxels belonging to the circular ring are almost doubled. Furthermore, the contrast between the more central and stronger paths and the surrounding weaker paths is enhanced with the 5x5x5 neighbourhood. However, in both Fig. 3a and Fig. 3b, we can identify the 7 central anisotropic voxels that have much greater FC values compared to the isotropic voxels that surround them. Fig. 2 and 3 suggest that FCT can differentiate regions that exhibit coherent fibre structure from non-coherent ones.

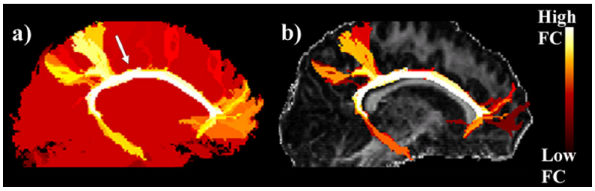

Fig. 4. a) Maximum intensity projection (MIP) of fuzzy connectedness values along the sagittal plane, for a seed ROI within the cingulum. The white arrow indicates the position of the seed. b) Thresholded MIP of FC values superimposed on a sagittal FA image. FC values are colour-coded.

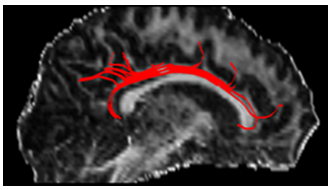

Fig. 5. Saggital view of streamlines generated from a seed ROI within the cingulum, similar to the seed used in Fig. 4. Streamlines are superimposed on a saggital FA image.

B. Human In-vivo Images

FCT was also applied to human brain images. Typical execution times using the 5x5x5 neighbourhood were in the order of 20 seconds on a 3.2 GHz PC. Fig. 4 shows FC maps when a coronal seed ROI within the cingulum was used. Fig. 4a shows a maximum intensity projection (MIP) of the raw FC values along the sagittal plane. In Fig. 4b (and for the rest of the results presented in this paper) a threshold has been applied to the FC values to keep only the most relevant voxels with the top 5% FC values and aid visualization. The results are superimposed on a saggital FA slice. We can observe, that the identified paths go correctly along the cingulate gurus and reach the hippocampus [10]. The streamlines generated from the same seed ROI are shown in Fig. 5. The streamlines are stopped at the level of the splenium of the corpus callosum and cannot reach the hippocampus. On the other hand, due to its distributed nature FCT goes through the relatively weak connections at the splenium level (evident by the reduction of the FC values) and reach the appropriate nucleus.

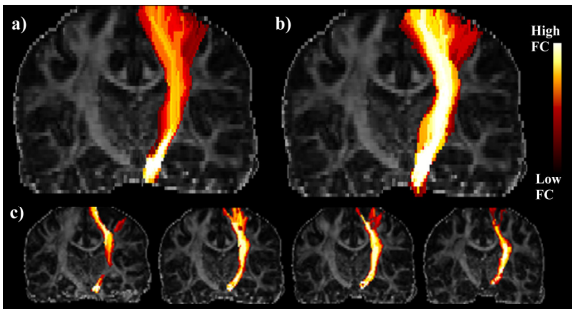

Fig. 6. Color-coded fuzzy connectedness values for the corticospinal tract generated using FCT and a seed ROI at the level of the pons. FC values are superimposed on coronal FA maps. a, b) Maximum intensity projections of thresholded FC values generated using a) a 3x3x3 and b) a 5x5x5 neighbourhood. c) Different coronal slices of FC values generated using a 5x5x5 neighbourhood.

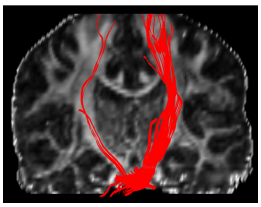

Fig. 7. Coronal view of streamlines generated from a seed ROI within the corticospinal tract, similar to the seed used in Fig. 6. Streamlines are superimposed on a coronal FA image.

Fig. 6 shows FC values for the corticospinal tract, when a seed ROI at the level of the pons in the right hemisphere is used. The maximum intensity projections (MIPs) of Fig. 6a and 6b show the less discrete nature of the results and the increased FC values obtained when increasing the neighbourhood size. The streamlines generated using the same seed are shown in Fig 7. In all cases, we can observe the greater fanning the paths exhibit to the motor cortex compared to the streamlines. This is due to the ability of the algorithm to consider tract branching, as shown in different coronal slices in Fig. 6c, where branching can be observed. Furthermore, streamline tractography gives rise to false positives, since wrongly connects the right corticospinal tract to the left motor cortex (Fig. 7). This is due to partial volume effects that occur at the pons because of the crossing of the corticospinal tract and the transverse pontine fibres [10]. FCT does not give rise to high connectedness paths to the left motor cortex, avoiding thus these false positives.

The distributed nature of FCT is further illustrated in Fig. 8, where single seed voxels are used. In Fig. 8a the seed voxel is placed in the fornix close to the septum. FC values indicate paths that agree well with a-priori anatomical knowledge [10]. Despite being a very high curved tract, the fornix is identified and can be differentiated from the background, which is thresholded and not shown. We can observe that apart from the main core of the fornix, some paths are identified at the level of the splenium of the corpus callosum that go posteriorly. Clearly these are false positives, however they are given a lower FC value than the core of the tract. In Fig. 8b, the seed voxel is placed in the genu of the corpus callosum and many callosal paths are

correctly identified. We can observe the many branching paths that are fanning out of the seed.

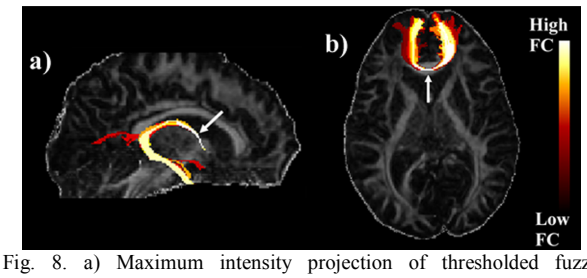

Fig. 8. a) Maximum intensity projection of thresholded fuzzy connectedness values along the sagittal plane, for a single seed voxel within the fornix. b) Maximum intensity projection of thresholded fuzzy connectedness values along the axial plane, for a single seed voxel in the genu of the corpus callosum. Results are superimposed on FA images. The white arrows indicate the position of the seeds.

Apart from connectedness values, FCT can provide the strongest paths that arise from a given seed. Fig. 9a presents the top 0.5% paths generated using FCT from a seed ROI in the splenium of the corpus callosum. Paths are generated by finding the voxels with the top 0.5% FC values and then propagating backwards to the seed. For each voxel belonging to a path, the principal eigenvector is plotted. Streamlines generated from the same seed are shown in Fig. 9b. We can observe that FCT paths exhibit greater branching.

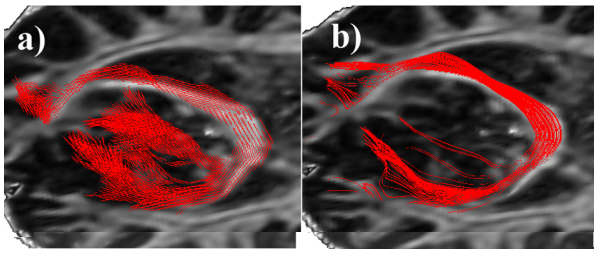

Fig. 9. a) Top 0.5% paths generated using FCT from a seed ROI in the splenium of the corpus callosum. b) Streamlines generated using the same ROI. Paths are superimposed on axial FA images.

IV. Discussion

We have presented a new fuzzy approach for studying brain anatomical connectivity using diffusion MRI. The FCT algorithm checks all possible paths, as these are defined on the discrete image grid, between any pair of voxels in order to assign them a global connectivity index. This assignment is done by using a local voxel similarity measure, which depends on the fibre orientation estimates in each voxel. Under the assumption that WM tracts should exhibit relatively strong orientational coherence, paths belonging to the same tract are given a high strength and can be differentiated from the background (e.g. Fig. 2, Fig. 4a).

Our technique produced distributed and fuzzy connectivity maps, contrary to streamline tractography that produces binary connectivity indices. For different seed regions in a healthy brain, results agreed well with a priori anatomical knowledge [10]. For all tracts shown, FCT assigned high connectivity values to voxels belonging to the main core of the tract. False positive connections are possible, especially in cases of highly curved tracts, such as the fornix. In Fig. 8 the fornix appears to be connected to some tracts running posteriorly to the cortex. However, these false positives were in general characterized by lower FC values. Given the difficulty of validating tractography methods in living individuals, we showed the performance of FCT to simulated data, as well as to real data in regions where an anticipated answer exists. In the simulations presented in Fig. 2, FCT correctly identified the region with structural coherence and differentiate it from the isotropic non-coherent background.

FCT is a fast algorithm that effectively finds the weakest link of the strongest path connecting two points. This link will determine the strength of the path. Similar connectivity indices have been introduced by other techniques, such as fast marching tractography [15] and front evolution tractography [16], which assign connectivity values based on the weakest link of paths. The former utilizes a map of front arrival times and the latter evolves a surface in 3D space. Fuzzy connectedness inherently searches for these weakest points. Compared to probabilistic tractography methods [13, 14], FCT is faster (seconds vs minutes of execution) and also its connectivity index does not depend on the distance from the seed point. This is a drawback of probabilistic methods, where the connectivity index is defined as the product of transition probabilities between consecutive points of a path [13, 14]. The longer the path, the smaller this product will be. A recent method that uses Dijkstra's algorithm and graph theory to perform distributed tractogtaphy [23] has also a similar problem, since it uses the product of transition probabilities as a connectivity index. However, the current implementation of FCT is not directly comparable to the probabilistic methods that utilize the uncertainty in the orientation estimates. Further validation of FCT and direct comparison with other tractography techniques is needed and we are currently working towards this direction.

FCT inherently considers path branching (Fig. 6, Fig. 9), which is a major limitation of streamline approaches. However, the degree to which branching will be considered depends on the affinity function. The affinity utilized here causes a reduction of the connectivity when branching occurs. An affinity adaptable to the tensor eigenvalues should modify FC values in branching regions to reflect the data, rather than just the method.

In this study, we used a voxel similarity measure based on the diffusion tensor principal eigenvector. Incorporating other similarity measures is straightforward, as FCT is independent of the affinity function utilized. Using uncertainty in the orientation estimates [13, 14], multiple fibre orientations per voxel [22, 24] and incorporating curvature in the affinity are some direct extensions of this work that should improve FCT performance.

In the current FCT implementation path propagation occurs only between voxel centres. Streamline tractography provides smoother paths since it does not necessarily connect voxel centres (Fig. 9). However, the adopted path plotting

scheme used in Fig. 9 for FCT is very simple and smoother paths can be obtained using e.g. splines. Moreover, other ways to increase the algorithm's spatial continuity are currently explored and will be the subject of a future study.

APPENDIX

The FCT algorithm calculates fuzzy connectedness values $f(\mathbf{a})$ between every image voxel **a** and the seed voxel(s) **s.** FCT also outputs the **Memory** array that keeps for every voxel **a** its previous through which **a** is connected to the seed in a strongest way. Pairwise affinities μ between each voxel and its neighbours are used as input, while a queue is used as an auxiliary structure. Pseudo-code is provided below, for the case of a 3x3x3 neighbourhood. In the case of a 5x5x5 neighbourhood, modifications of the conditional branch between lines 14-20 should be made according to the algorithm description of Section IIB.

```
1: f(a)=0;   Memory(a)=undefined, for every image voxel a
2: f(s)=1;   Enqueue(s), for every seed voxel s
3:  While (Queue!=empty)
4:     Dequeue(i) with maximum f value;
5:     prev=Memory(i);
6:     For each neighbour j of i
7:        fmin=min(f(i),μ(i,j));
8:        If (prev!=undefined)
9:              Compute vectors n1=i-prev and n2=j-i;
10:             Compute dot product dot=n1n2;
11:             If (dot<=0) fmin=0;
12:             End If;
13:       End If;
14:       If (fmin>f(j))
15:             f(j)=fmin;
16:             Memory(j)=i;
17:             If (j is not in queue) Enqueue(j);
18:             Else Update f(j);
19:             End If;
20:       End If;
21:   End For;
22:  End While;
```


ACKNOWLEDGMENT

We would like to thank Dr. Paul S. Morgan from the Division of Academic Radiology at the University of Nottingham, UK for generously providing the MRI data. Also, Prof. Jayaram K. Udupa from the Department of Radiology at the University of Pennsylvania, USA for stimulating discussions.

REFERENCES

[1] R. Bammer, "Basic principles of diffusion-weighted imaging," *Eur J Radiol,* vol. 45, pp. 169-84, 2003.

[2] C. Beaulieu, "The basis of anisotropic water diffusion in the nervous system - a technical review," *NMR Biomed,* vol. 15, pp. 435-55, 2002.

[3] P. J. Basser, S. Pajevic, C. Pierpaoli, J. Duda, and A. Aldroubi, "In vivo fiber tractography using DT-MRI data," *Magn Reson Med,* vol. 44, pp. 625-32, 2000.

[4] S. Mori, B. J. Crain, V. P. Chacko, and P. C. van Zijl, "Three-dimensional tracking of axonal projections in the brain by magnetic resonance imaging," *Ann Neurol,* vol. 45, pp. 265-9, 1999.

[5] P. J. Basser, "Inferring microstructural features and the physiological state of tissues from diffusion-weighted images," *NMR Biomed,* vol. 8, pp. 333-44, 1995.

[6] C. Pierpaoli, P. Jezzard, P. J. Basser, A. Barnett, and G. Di Chiro, "Diffusion tensor MR imaging of the human brain," *Radiology,* vol. 201, pp. 637-48, 1996.

[7] D. C. Alexander, "An introduction to computational diffusion MRI: the diffusion tensor and beyond," in *Visualization and Processing of Tensor Fields*, J. Weickert and H. Hagen, Eds. Berlin Heidelberg: Springer, 2006, pp. 83-106.

[8] D. C. Alexander, "Multiple-fiber reconstruction algorithms for diffusion MRI," *Ann N Y Acad Sci,* vol. 1064, pp. 113-33, 2005.

[9] P. J. Basser, J. Mattiello, and D. LeBihan, "Estimation of the effective self-diffusion tensor from the NMR spin echo," *J Magn Reson B,* vol. 103, pp. 247-54, 1994.

[10] S. Mori, S. Wakana, P. C. Van Zijl, and L. M. Nagae-Poetscher, *MRI Atlas of Human White Matter*: Elsevier, 2005.

[11] S. P. Awate, H. Zhang, and J. C. Gee, "A fuzzy, nonparametric segmentation framework for DTI and MRI analysis: with applications to DTI-tract extraction," *IEEE Trans Med Imaging,* vol. 26, pp. 1525-36, 2007.

[12] J. K. Udupa and S. Samarasekera, "Fuzzy Connectedness and Object Definition: Theory, Algorithms, and Applications in Image Segmentation," *Graphical Models and Image Processing,* vol. 58, pp. 246-261, 1996.

[13] T. E. Behrens, M. W. Woolrich, M. Jenkinson, H. Johansen-Berg, R. G. Nunes, S. Clare, P. M. Matthews, J. M. Brady, and S. M. Smith, "Characterization and propagation of uncertainty in diffusion-weighted MR imaging," *Magn Reson Med,* vol. 50, pp. 1077-88, 2003.

[14] O. Friman, G. Farneback, and C. F. Westin, "A Bayesian approach for stochastic white matter tractography," *IEEE Trans Med Imaging,* vol. 25, pp. 965-78, 2006.

[15] G. J. Parker, C. A. Wheeler-Kingshott, and G. J. Barker, "Estimating distributed anatomical connectivity using fast marching methods and diffusion tensor imaging," *IEEE Trans Med Imaging,* vol. 21, pp. 505-12, 2002.

[16] J. D. Tournier, F. Calamante, D. G. Gadian, and A. Connelly, "Diffusion-weighted magnetic resonance imaging fibre tracking using a front evolution algorithm," *Neuroimage,* vol. 20, pp. 276-88, 2003.

[17] S. N. Sotiropoulos, C. R. Tench, and L. Bai, "Fuzzy Anatomical Connectedness using Diffusion MRI: An Approach to Tractography of the Brain," in *ISMRM Meeting*, Toronto, Canada, 2008, p. 1846.

[18] L. G. Nyul, A. X. Falcao, and J. K. Udupa, "Fuzzy-connected 3D image segmentation at interactive speeds," *Graphical Models,* vol. 64, pp. 259-281, 2003.

[19] C. Poupon, C. A. Clark, V. Frouin, J. Regis, I. Bloch, D. Le Bihan, and J. Mangin, "Regularization of diffusion-based direction maps for the tracking of brain white matter fascicles," *Neuroimage,* vol. 12, pp. 184-95, 2000.

[20] D. K. Jones, "Determining and visualizing uncertainty in estimates of fiber orientation from diffusion tensor MRI," *Magn Reson Med,* vol. 49, pp. 7-12, 2003.

[21] P. B. Kingsley, "Introduction to diffusion tensor imaging mathematics: Part III. Tensor calculation, noise, simulations, and optimization," *Concepts in Magnetic Resonance Part A,* vol. 28A, pp. 155-179, 2006.

[22] S. N. Sotiropoulos, L. Bai, P. S. Morgan, D. P. Auer, C. S. Constantinescu, and C. R. Tench, "A Regularized Two-Tensor Model Fit to Low Angular Resolution Diffusion Images Using Basis Directions," *Journal of Magnetic Resonance Imaging,* vol. *28*, pp. 199-209, 2008.

[23] A. Zalesky, "DT-MRI Fiber Tracking: A Shortest Paths Approach," *IEEE Trans Med Imaging,* vol. in press, 2008.

[24] D. S. Tuch, "Q-ball imaging," *Magn Reson Med,* vol. 52, pp. 1358-72, 2004.